

Across-strike asymmetry of the Andes orogen linked to the age and geometry of the Nazca plate

Pedro Val* and Jane K. Willenbring†

Scripps Institution of Oceanography, University of California San Diego, La Jolla, California 92093, USA

ABSTRACT

The crest of the Andes—the trace of the highest mountain topography—weaves back and forth, in places near the coastline, in others farther inland. Its position reflects the asymmetric distribution of orogen mass and coincides with asymmetry of orographic precipitation. This coincidence is thought to reflect a primary influence of orographic precipitation on accumulated orogenic mass whereby the more erosive (wetter) side promotes crest migration toward the less erosive (drier) side. However, whether this remains the case after excluding tectonic controls on the size and asymmetry of the wedge is an open question. We assessed relationships between precipitation, erosion rates, and the macromorphology of the Andes. We find that precipitation rates cannot sufficiently explain orogen asymmetry after statistically controlling for the age or dip of the Nazca slab. Slab age and dip are known to primarily affect mountain building in the Andes by impacting stress and strain propagation into the retro-arc region, thus better explaining the position of the mountain chain within the orogenic wedge. Accordingly, using basin-wide erosion rate, topographic, and precipitation data, we find that precipitation possibly influences erosional efficiency in semi-arid Andean landscapes but falls short in explaining the variability of erosion rates in regions of high orographic precipitation. We conclude that the orographic effect cannot change the Andean macromorphology that is set by bottom-up tectonic processes.

INTRODUCTION

The across-strike asymmetry of orogens is rooted in tectonically imposed spatial gradients in lateral and vertical rock advection (Willett et al., 1993). As mountains grow and develop orographic-precipitation effects, high precipitation rates on the wet side are thought to force mountain range asymmetry by increasing the erosional efficiency and driving mountain crest migration toward the dry side (Willett, 1999). In the Andes orogen (Fig. 1), orographic effects have sustained extreme precipitation gradients since Miocene times (Mulch et al., 2010; Insel et al., 2012). Their coincidence with systematic variations in crustal shortening, exhumation, and across-strike asymmetry of orogen mass has been attributed to a first-order control of orographic precipitation on asymmetric ero-

sion (Masek et al., 1994; Horton, 1999; Montgomery et al., 2001; Strecker et al., 2007; Mora et al., 2008). However, in orogens bounded by subduction zones, the properties and dynamics of the subducting slab (i.e., age and geometry) partly control the spatial distribution of strain and uplift in the upper plate (Jordan et al., 1983; Gephart, 1994; Ouimet and Cook, 2010; Capitanio et al., 2011; Horton, 2018). An open question we address is: How much of the across-strike asymmetry along the Andes is rooted in these tectonic drivers compared to precipitation distribution?

Decoupling the purported climatically driven orogenic asymmetry from tectonic control is a difficult task because there are few techniques or proxies for constraining the lateral advection of rocks in large orogens such as the Andes (e.g., Eizenhöfer et al., 2019). We approach this question by seeking evidence of the diagnostic relationships between topography, erosion rates, precipitation rates, and across-strike asymmetry as predicted by fluvial incision and critical taper theories. The Andes provide a unique natural laboratory given the geometries and age range of

subducting slabs that are found in sections of the continent where winds originate from the west or the east, allowing a separation of the effects of tectonics and direction of the orographic effect. Using data on the age and geometry of the Nazca slab as proxies for tectonic controls over orogenic wedge evolution and pro-wedge and retro-wedge precipitation rates, we statistically assessed the partitioning between tectonic and climatic contributions to orogen asymmetry. We used a compilation of 375 basin-wide erosion rates to assess the statistical findings based on bedrock fluvial incision theory.

End-Member Predictions of Orogen Asymmetry

Fluvial incision theory predicts that higher precipitation rates increase erosional efficiency and decrease the steady-state topographic steepness required for a given uplift rate (e.g., Whipple, 2009). This topographic feedback can change orogenic asymmetry by driving mountain crest migration but only under spatially uniform uplift rates (e.g., Goren et al., 2014). If predetermined by a tectonic uplift gradient, only extreme orographic effects such as in the Andes can impact but not reverse an orogen's asymmetry (Willett, 1999; Goren et al., 2014).

From critical taper theory, high erosional efficiency reduces or limits the total and retro-wedge widths for a given tectonic accretionary flux (Dahlen, 1990), which necessarily accelerates rock uplift rates (Whipple, 2009). If orographic precipitation drives this positive feedback, the diagnostic evidence would be high erosion rates and reduced orogenic widths coinciding with regions of high orographic precipitation (Whipple and Meade, 2004). Given the east-verging nature of the Andes growth, high erosional efficiency and precipitation rate in the pro-wedge is expected to favor pro-wedge widening, whereas high erosional efficiency in the retro-wedge should limit the propagation of the deformation front (Horton, 1999; Willett,

*Current address: Department of Geology, School of Mines, Federal University of Ouro Preto, Ouro Preto, MG, 35400-00, Brazil; E-mail: pedroval07@gmail.com.

†Current address: Department of Geological Sciences, Stanford University, Stanford, California 94305, USA.

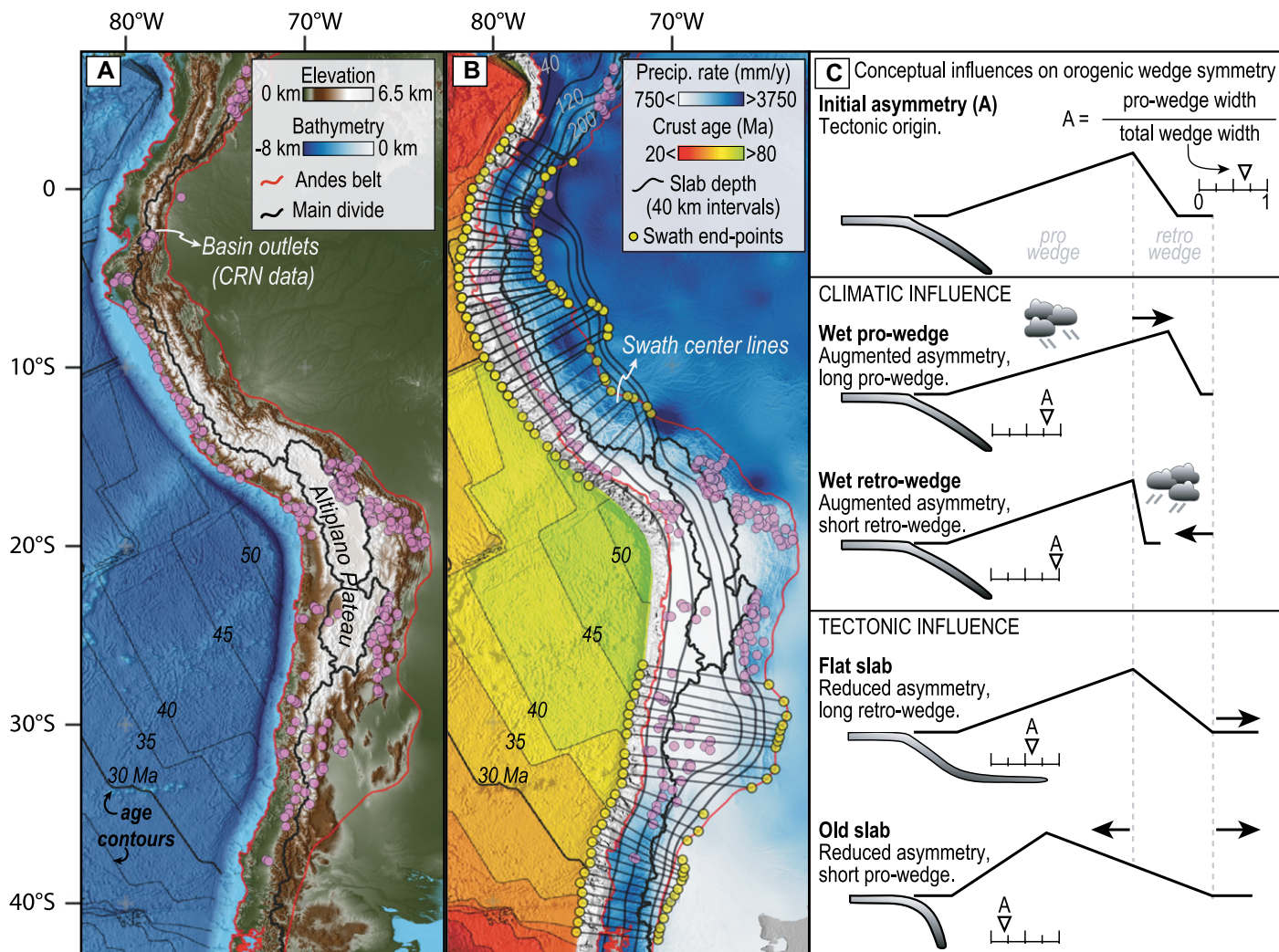


Figure 1. Study area and conceptual models of orogenic wedge forcing. (A) Elevation along the Andes from the trench to retro-wedge deformation front (red bold line) and watershed outlets (purple circles) of basins containing erosion rate data derived from cosmogenic radionuclides (CRN). (B) 34 yr mean annual precipitation (Precip.) rate map for the Andes (Karger et al., 2017), oceanic crust age contours (Seton et al., 2020), slab depth contours (Hayes et al., 2018), and location of swath profiles (black across-strike lines). (C) Conceptual models of climatic forcing of an orogenic wedge shape shown as width (Whipple and Meade, 2004; Whipple, 2009) and taper (Willett, 1999) adjustments. Also shown are conceptual models of subduction zone forcing of an orogenic wedge shape inspired by previous studies (Jordan et al. 1983; Capitanio et al., 2011; Horton, 2018).

1999; McQuarrie et al., 2008). If orographic precipitation is the principal driver of orogenic asymmetry in the Andes, the retro-wedge width should be systematically narrower and the orogen systematically more asymmetric (Fig. 1C). In this study, we assessed these diagnostic relationships in the Andes mountains.

METHODS

We used multilinear models to statistically assess the partial tectonic and climatic contributions to orogen asymmetry. In a convergent margin, the subduction zone megathrust balances the forces in the subduction zone–orogen interface (Meade and Conrad, 2008). Thus, orogen asymmetry is calculated as the ratio of trench-orthogonal distances from the trench to the peak mean topography (i.e., pro-wedge) and from the trench to the retro-wedge deformation front (i.e.,

total width). A value of 0.5 reveals a symmetrical orogen, and values below or above 0.5 reveal a narrower or wider pro-wedge, respectively. We positioned the deformation front according to the geologic map of South America (Gómez et al., 2019) and corrected to include retro-wedge basement uplifts in Peru and Argentina (Fig. 1; Text S1 in the Supplemental Material¹). The average position of the crest was identified in 100-km-wide, approximately trench-normal topographic swath profiles over an ~500-m-resolution digital elevation model (DEM) (Tozer

¹Supplemental Material. Datasets, regression data, and descriptions of minor corrections to the datasets, and a detailed description of the statistical methods. Please visit <https://doi.org/10.1130/GEOL.S.20504514> to access the supplemental material, and contact editing@geosociety.org with any questions.

et al., 2019) by averaging the location of the highest 1% peaks in mean elevation (Fig. 1; Fig. S1). We excluded the Altiplano-Puna plateau given that its crustal deformation reflects ductile behavior and lateral crustal flow (e.g., Ouimet and Cook, 2010) and likely deviates from the critical taper predictions for orogenic wedges.

We used multilinear models of the form $Y = r + \beta_1 X_1 + \beta_2 X_2$, where Y is orogen asymmetry, r are the model residuals, X_1 and X_2 are predictors of Y (as described below), and β_1 and β_2 are the regression coefficients (the regression slopes). At-trench slab age (Seton et al., 2020) and slab dips (0–125 km depth) (Hayes et al., 2018) of the Nazca slab are two metrics we used as the tectonic predictors, based on the literature (Capitanio et al., 2011; Horton, 2018). For climatic predictors, we used modal pro- and retro-wedge precipitation rates from a 34 yr annual

average precipitation rate data set (1 km resolution; Karger et al., 2017) (Figs. S2 and S3). Four models use a tectonic predictor (slab age or slab dip as X_1) and a climatic predictor (pro- or retro-wedge precipitation rate as X_2). A fifth model uses slab age as X_1 and slab dip as X_2 . Predictors were centered at a mean of 0 and normalized to a standard deviation to yield comparable regression slopes (β_1 and β_2) and inform the relative dependence of Y on X_1 and X_2 . The residuals and regression results were then used to detect nonlinear dependencies of Y on precipitation rates (see Text S2). Multilinear analysis requires linear correlations with the response variable. Thus, we used log slab dip and log precipitation rate for improved linearity. None of the X_1 - X_2 pairs used here are affected by severe collinearity (i.e., $R^2 > 0.8$).

We used previously compiled basin-wide erosion rates (Codilean et al., 2018), morphometric averages (hillslope gradient and river steepness, k_{sn}), and average precipitation rates (Karger et al., 2017) to assess potential precipitation-erosion rate links in 375 basins (see Text S3). We extracted basin-wide top-

ographic data from 90 m and 30 m DEMs (NASA, 2013) for basins greater and smaller than 5 km², respectively, using topographic tools (Schwanghart and Scherler, 2014; Forte and Whipple, 2019). We explored potential climatic imprints on erosion rates using the enhanced river steepness ($k_{sn}q$), a metric that accounts for climate using river discharge, q (computed as precipitation \times the in-stream flow accumulation grid). If climate influences erosional efficiency, $k_{sn}q$ should correlate with erosion rates better than k_{sn} (Adams et al., 2020).

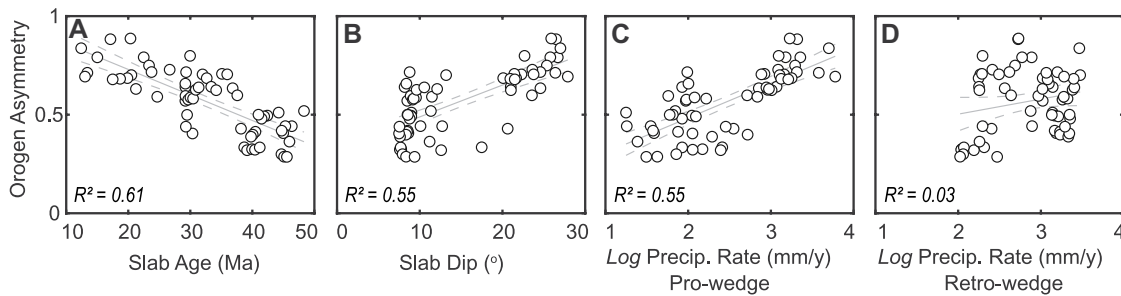
The time span of the precipitation rate data set used here is undoubtedly short compared to the time scales of cosmogenic nuclide integration (10²–10⁵ yr) and mountain building (10⁷ yr). However, the orographic-precipitation effects and thus the relative spatial distribution of precipitation rates are long-lasting features of the Andes and established at least since the Miocene (Strecker et al., 2007; Mulch et al., 2010; Insel et al., 2012). Thus, basin-wide averages likely reflect the long-term differences between the studied regions. Lastly, any possibility of ¹⁰Be

erosion rates having been reset by past climate (e.g., Insel et al., 2010) is likely diluted in the large data set ($n = 375$).

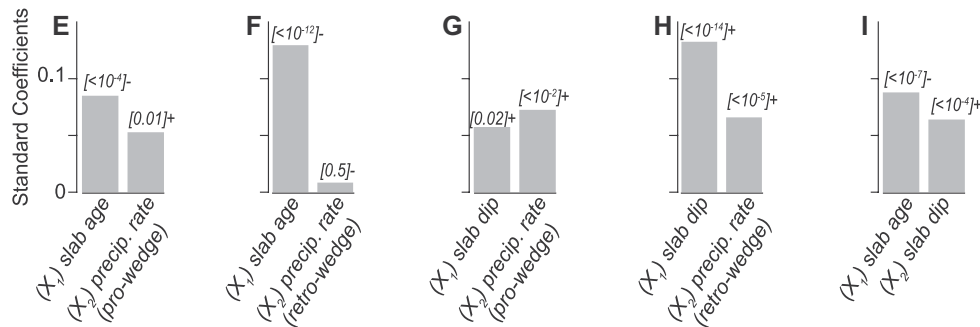
RESULTS

Orogen asymmetry in the Andes varies between 0.29 and 0.89 and is correlated negatively with slab age and positively with slab dip and pro-wedge precipitation rate, and not correlated with retro-wedge precipitation rate (Fig. 2). Slab age alone explains 61% of the variability in orogen asymmetry, followed by slab dip and pro-wedge precipitation rates (each 55%). The directions of the observed relationships are consistent with scenarios in which each parameter individually influences the asymmetry (Figs. 1C and 2A–2D). Multilinear models composed of tectonic and climatic variables explain 65% of the variability in orogenic asymmetry but do not represent a significant improvement from the univariate model using slab age (Figs. 2A and 2E). The fully tectonic model (i.e., slab age as X_1 and slab dip as X_2) explains 70% of the variability in orogen asymmetry. Precipitation rates are, therefore, secondary predictors at best.

(A–D) Bivariate Relationships



(E–I) Standardized Multilinear Models



(J–M) Partial Relationships with Precipitation

(Y is adjusted to X_1 , where X_1 is slab age (J, K) or dip (L, M))

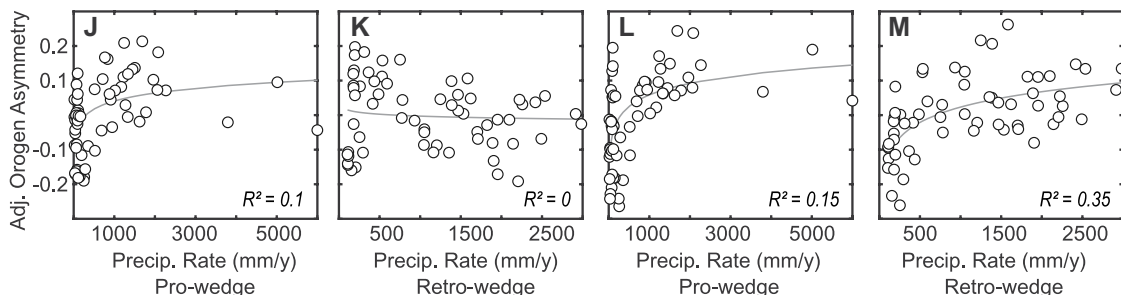


Figure 2. Tectonic and climatic relationships with orogenic asymmetry. (A–D) Correlations between orogen asymmetry and slab age at trench (p -value < 0.001) (A), slab dip (p -value < 0.01) (B), pro-wedge precipitation rate (p -value < 0.01) (C), and retro-wedge precipitation rate (p -value = 0.09) (D) measured in swath profiles (see swath centerlines in Fig. 1B). Residuals of linear regressions approximate normal distributions. Summary statistics are presented in Table S1 (see footnote 1). (E–I) Regression slopes (β_1 and β_2 in each model; see text) of multilinear models (Table S2). X_1 and X_2 are predictors of orogen asymmetry (Y). Numbers in brackets indicate the p -value of a given coefficient, and positive and negative signs indicate slope of relationship in the model. (J–M) Partial residual plots showing Y adjusted to X_1 (e.g., $Y_{adj} = r + \beta_2 X_2$) versus X_2 for four models using climatic and tectonic variables. Gray lines show partial regressions (Table S3).

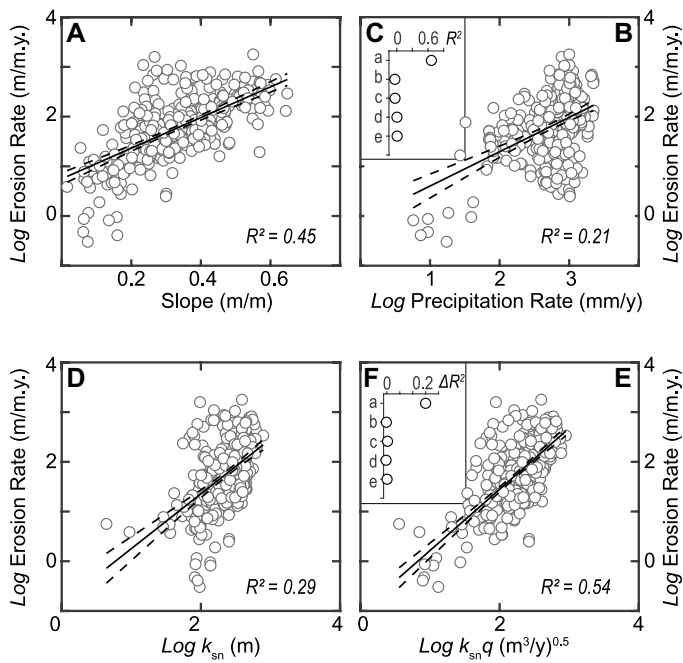


Figure 3. Basin-wide erosion rates, hillslope gradients, and relationships with climate. (A,B) Erosion rates plotted against hillslope gradient (A) and log precipitation rate (B). (C) Adjusted R^2 for regressions of erosion rate versus precipitation rate separated by precipitation bins a–e (a–d: intervals of 250 mm/y up to 1250 mm/y; e: >1250 mm/y). (D,E) Erosion rates plotted against river steepness, k_{sn} (D) and $k_{sn}q$ (E). (F) Improvement on erosion- k_{sn} relationship shown as difference in R^2 between $k_{sn}q$ and k_{sn} (ΔR^2) in each precipitation bin as defined in C. Data are basin-wide averages (see outlet locations in Fig. 1).

Slab age and dip have higher regression slopes in all the models tested and thus are more important predictors of orogen asymmetry than pro- or retro-wedge precipitation rates (Figs. 2E–2I). Albeit weakly, orogen asymmetry is nonlinearly related to pro-wedge precipitation after adjusting for slab age (Fig. 2J). Here, regression slopes are steepest at pro-wedge precipitation rates <~500 mm/y. This is also true for pro- and retro-wedge precipitation adjusted to slab dip (Figs. 2L and 2M). Beyond ~500 mm/y, the nonlinear slopes are insignificant and reveal that high orographic precipitation rates have no statistical effect on orogen asymmetry.

Erosion rates are weakly correlated with precipitation rates, moderately correlated with river steepness (k_{sn}), and mostly explained by hillslope gradients ($R^2 \sim 45\%$) (Figs. 3A and 3B). Dividing the data into precipitation bins reveals no systematic increase in erosion rate (Figs. 3B and 3C), contrary to what would be expected if precipitation rates had limited the growth of the orogen. We observe a statistically significant improvement in the regression against erosion rate going from k_{sn} ($R^2 = 0.29$) to $k_{sn}q$ ($R^2 = 0.54$) (Figs. 3D and 3E). The improvement is greatest for the driest basins (precipitation of 0–250 mm/y) but insignificant for wetter ones (Fig. 3F). This observation lends process-based empirical support to the statistical observations.

IMPLICATIONS

Slab ages are nearly symmetrical about the Altiplano-Puna plateau and describe across-strike orogen asymmetry in a statistically significant, unifying trend (Fig. 2A). This observation suggests a primary control of orogen asymmetry

rooted in the subduction zone. Older segments of the subducting Nazca slab require a thicker crust in the South American plate to balance tectonic forces with high vertical stresses near the trench (Capitanio et al., 2011). In areas next to an older slab (and thicker continental crust), compressive forces propagate further into the orogen over time and drive retro-wedge growth (Capitanio et al., 2011). The wedge width data presented herein suggests this process leads to greater accumulation of mass in the retro-wedge area (Fig. 2A; Fig. S3) and is evident in the across-strike profiles along the Andes (Fig. 4). That slab dip can also partly explain orogen asymmetry suggests it is of secondary importance compared to slab age, consistent with previous studies (Jordan et al., 1983; Gephart, 1994; Capitanio et al., 2011; Horton, 2018).

Changes in the slab shape and age accompany changes in the force balance of the subduction zone as well as the shape of the mantle wedge and lithosphere-asthenosphere boundary underneath the orogen, all of which form a bottom-up control on the direction of tectonic transport and orogen structure (Schellart, 2017; Barrionuevo et al., 2021). Together with our results, this mechanism suggests that the orogenic wedge asymmetry in non-collisional orogens is subject to subduction zone dynamics.

The spatial coincidence of heavy orographic effects and asymmetric mass distribution along the Andes orogen have long been thought to originate in its sustained control on precipitation distribution (e.g., Horton, 1999; Montgomery et al., 2001; McQuarrie et al., 2008). Our analysis of $k_{sn}q$ -erosion relationships and statistical observations suggests that precipitation influences erosional efficiency mostly in

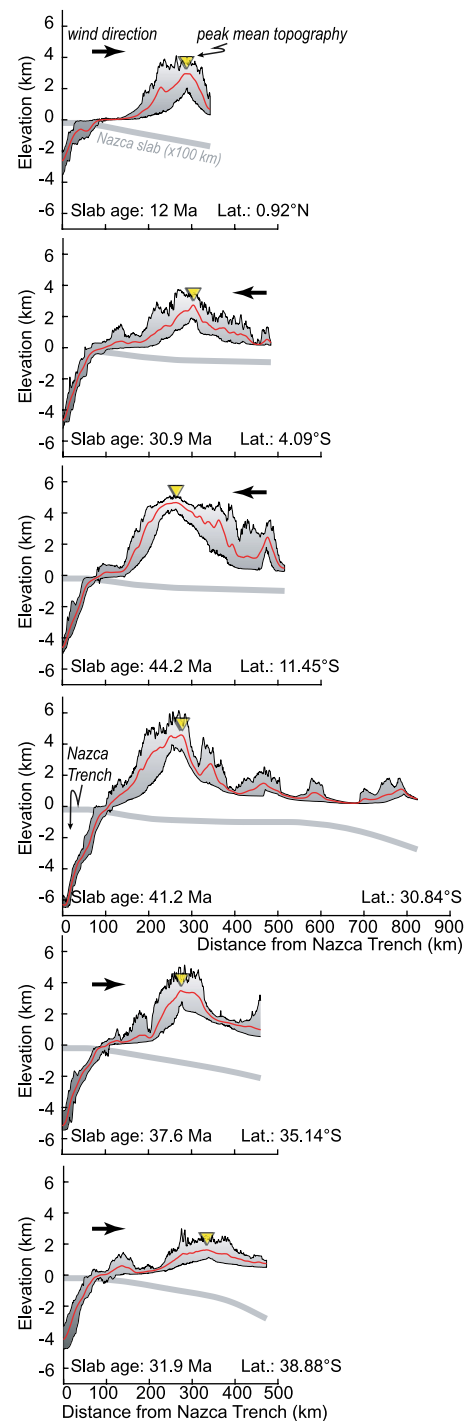


Figure 4. Trench-normal, 100-km-wide swath topographic and bathymetric profiles at six locations along strike of the Andes orogenic wedge. Wind direction is shown (large arrow) and indicates the side of the Andes that receives the most precipitation. Location of the peak mean topography is shown (triangle). Depth of top of slab (bold gray line) is 100× the bathymetry scale. All swath profiles are provided in the Supplemental Material (see footnote 1).

drier regions but not otherwise (Fig. 3F). These results reveal that it is at precipitation rates <~500 mm/y that precipitation changes more likely influence erosional efficiency and orogen

shape (Figs. 2J–2M). This nonlinear dependence on climate may be related to critical erosion thresholds, which are more likely exceeded in drier climates (e.g., DiBiase and Whipple, 2011). We conclude that high orographic precipitation has minimal influence on erosional efficiency and, therefore, cannot drive changes in wedge widths, which are set by bottom-up tectonic processes. Unlike previously thought (Montgomery et al., 2001), the influence of climate on the asymmetry of the Andes is limited and, therefore, not primary.

ACKNOWLEDGMENTS

P. Val was funded by the U.S. National Science Foundation (award 1651243 to J.K. Willenbring). We thank F. Capitanio, K. Murray, N. Perez, S. Willett, and three anonymous reviewers. We also thank H. Reis, N. Lyons, and D. Peifer for insightful discussions.

REFERENCES CITED

- Adams, B.A., Whipple, K.X., Forte, A.M., Heimsath, A.M., and Hodges, K.V., 2020, Climate controls on erosion in tectonically active landscapes: *Science Advances*, v. 6, eaaz3166, <https://doi.org/10.1126/sciadv.aaz3166>.
- Barrionuevo, M., Liu, S.B., Mescua, J., Yagupsky, D., Quinteros, J., Giambiagi, L., Sobolev, S.V., Piceda, C.R., and Strecker, M.R., 2021, The influence of variations in crustal composition and lithospheric strength on the evolution of deformation processes in the southern Central Andes: Insights from geodynamic models: *International Journal of Earth Sciences*, v. 110, p. 2361–2384, <https://doi.org/10.1007/s00531-021-01982-5>.
- Capitanio, F.A., Faccenna, C., Zlotnik, S., and Stegman, D.R., 2011, Subduction dynamics and the origin of Andean orogeny and the Bolivian orocline: *Nature*, v. 480, p. 83–86, <https://doi.org/10.1038/nature10596>.
- Codilean, A.T., Munack, H., Cohen, T.J., Saktura, W.M., Gray, A., and Mudd, S.M., 2018, OCTOPUS: An open cosmogenic isotope and luminescence database: *Earth System Science Data*, v. 10, p. 2123–2139, <https://doi.org/10.5194/essd-10-2123-2018>.
- Dahlen, F.A., 1990, Critical taper model of fold-and-thrust belts and accretionary wedges: *Annual Review of Earth and Planetary Sciences*, v. 18, p. 55–99, <https://doi.org/10.1146/annurev.earth.18.050190.000415>.
- DiBiase, R.A., and Whipple, K.X., 2011, The influence of erosion thresholds and runoff variability on the relationships among topography, climate, and erosion rate: *Journal of Geophysical Research*, v. 116, F04036, <https://doi.org/10.1029/2011JF002095>.
- Eizenhöfer, P.R., McQuarrie, N., Shelef, E., and Ehlers, T.A., 2019, Landscape response to lateral advection in convergent orogens over geologic time scales: *Journal of Geophysical Research: Earth Surface*, v. 124, p. 2056–2078, <https://doi.org/10.1029/2019JF005100>.
- Forte, A.M., and Whipple, K.X., 2019, Short communication: The Topographic Analysis Kit (TAK) for TopoToolbox: *Earth Surface Dynamics*, v. 7, p. 87–95, <https://doi.org/10.5194/esurf-7-87-2019>.
- Gephart, J.W., 1994, Topography and subduction geometry in the central Andes: Clues to the mechanics of a noncollisional orogen: *Journal of Geophysical Research*, v. 99, p. 12,279–12,288, <https://doi.org/10.1029/94JB00129>.
- Gómez, J., Schobbenhaus, C., and Montes, N.E., compilers, 2019, Geological map of South America 2019: Paris, Commission for the Geological Map of the World (CGMW), Colombian Geological Survey and Geological Survey of Brazil, scale 1:5,000,000, <https://doi.org/10.32685/10.143.2019.929>.
- Goren, L., Willett, S.D., Herman, F., and Braun, J., 2014, Coupled numerical-analytical approach to landscape evolution modeling: *Earth Surface Processes and Landforms*, v. 39, p. 522–545, <https://doi.org/10.1002/esp.3514>.
- Hayes, G.P., Moore, G.L., Portner, D.E., Hearne, M., Flamme, H., Furtney, M., and Smoczyk, G.M., 2018, Slab2, a comprehensive subduction zone geometry model: *Science*, v. 362, p. 58–61, <https://doi.org/10.1126/science.aat4723>.
- Horton, B.K., 1999, Erosional control on the geometry and kinematics of thrust belt development in the central Andes: *Tectonics*, v. 18, p. 1292–1304, <https://doi.org/10.1029/1999TC900051>.
- Horton, B.K., 2018, Tectonic regimes of the central and southern Andes: Response to variations in plate coupling during subduction: *Tectonics*, v. 37, p. 402–429, <https://doi.org/10.1002/2017TC004624>.
- Insel, N., Ehlers, T.A., Schaller, M., Barnes, J.B., Tawackoli, S., and Poulsen, C.J., 2010, Spatial and temporal variability in denudation across the Bolivian Andes from multiple geochronometers: *Geomorphology*, v. 122, p. 65–77, <https://doi.org/10.1016/j.geomorph.2010.05.014>.
- Insel, N., Poulsen, C.J., Ehlers, T.A., and Sturm, C., 2012, Response of meteoric $\delta^{18}O$ to surface uplift—Implications for Cenozoic Andean Plateau growth: *Earth and Planetary Science Letters*, v. 317–318, p. 262–272, <https://doi.org/10.1016/j.epsl.2011.11.039>.
- Jordan, T.E., Isacks, B.L., Allmendinger, R.W., Brewer, J.A., Ramos, V.A., and Ando, C.J., 1983, Andean tectonics related to geometry of subducted Nazca plate: *Geological Society of America Bulletin*, v. 94, p. 341–361, [https://doi.org/10.1130/0016-7606\(1983\)94<341:ATRTGO>2.0.CO;2](https://doi.org/10.1130/0016-7606(1983)94<341:ATRTGO>2.0.CO;2).
- Karger, D.N., Conrad, O., Böhner, J., Kawohl, T., Kreft, H., Soria-Auza, R.W., Zimmermann, N.E., Linder, H.P., and Kessler, M., 2017, Climatologies at high resolution for the Earth land surface areas: *Scientific Data*, v. 4, 170122, <https://doi.org/10.1038/sdata.2017.122>.
- Masek, J.G., Isacks, B.L., Gubbels, T.L., and Fielding, E.J., 1994, Erosion and tectonics at the margins of continental plateaus: *Journal of Geophysical Research*, v. 99, p. 13,941–13,956, <https://doi.org/10.1029/94JB00461>.
- McQuarrie, N., Ehlers, T.A., Barnes, J.B., and Meade, B., 2008, Temporal variation in climate and tectonic coupling in the central Andes: *Geology*, v. 36, p. 999–1002, <https://doi.org/10.1130/G25124A.1>.
- Meade, B.J., and Conrad, C.P., 2008, Andean growth and the deceleration of South American subduction: Time evolution of a coupled orogen-subduction system: *Earth and Planetary Science Letters*, v. 275, p. 93–101, <https://doi.org/10.1016/j.epsl.2008.08.007>.
- Montgomery, D.R., Balco, G., and Willett, S.D., 2001, Climate, tectonics, and the morphology of the Andes: *Geology*, v. 29, p. 579–582, [https://doi.org/10.1130/0091-7613\(2001\)029<0579:CTATMO>2.0.CO;2](https://doi.org/10.1130/0091-7613(2001)029<0579:CTATMO>2.0.CO;2).
- Mora, A., Parra, M., Strecker, M.R., Sobel, E.R., Hooghiemstra, H., Torres, V., and Jaramillo, J.V., 2008, Climatic forcing of asymmetric orogenic evolution in the Eastern Cordillera of Colombia: *Geological Society of America Bulletin*, v. 120, p. 930–949, <https://doi.org/10.1130/B26186.1>.
- Mulch, A., Uba, C.E., Strecker, M.R., Schoenberg, R., and Chamberlain, C.P., 2010, Late Miocene climate variability and surface elevation in the central Andes: *Earth and Planetary Science Letters*, v. 290, p. 173–182, <https://doi.org/10.1016/j.epsl.2009.12.019>.
- NASA (National Aeronautics and Space Administration), 2013, Shuttle Radar Topography Mission (SRTM) Global: Distributed by OpenTopography, <https://doi.org/10.5069/G9445JDF> (access May 2021).
- Ouimet, W.B., and Cook, K.L., 2010, Building the central Andes through axial lower crustal flow: *Tectonics*, v. 29, TC3010, <https://doi.org/10.1029/2009TC002460>.
- Schellart, W.P., 2017, Andean mountain building and magmatic arc migration driven by subduction-induced whole mantle flow: *Nature Communications*, v. 8, 2010, <https://doi.org/10.1038/s41467-017-01847-z>.
- Schwanghart, W., and Scherler, D., 2014, Short communication: TopoToolbox 2—MATLAB-based software for topographic analysis and modeling in Earth surface sciences: *Earth Surface Dynamics*, v. 2, p. 1–7, <https://doi.org/10.5194/esurf-2-1-2014>.
- Seton, M., Müller, R.D., Zahirovic, S., Williams, S., Wright, N.M., Cannon, J., Whittaker, J.M., Matthews, K.J., and McGirr, R., 2020, A global data set of present-day oceanic crustal age and seafloor spreading parameters: *Geochemical Geophysical Geosystems*, v. 21, e2020GC009214, <https://doi.org/10.1029/2020GC009214>.
- Strecker, M.R., Alonso, R.N., Bookhagen, B., Carrapa, B., Hillel, G.E., Sobel, E.R., and Trauth, M.H., 2007, Tectonics and climate of the southern central Andes: *Annual Review of Earth and Planetary Sciences*, v. 35, p. 747–787, <https://doi.org/10.1146/annurev.earth.35.031306.140158>.
- Tozer, B., Sandwell, D.T., Smith, W.H.F., Olson, C., Beale, J.R., and Wessel, P., 2019, Global bathymetry and topography at 15 arc sec: SRTM15+: *Earth and Space Science*, v. 6, p. 1847–1864, <https://doi.org/10.1029/2019EA000658>.
- Whipple, K.X., 2009, The influence of climate on the tectonic evolution of mountain belts: *Nature Geoscience*, v. 2, p. 97–104, <https://doi.org/10.1038/ngeo413>.
- Whipple, K.X., and Meade, B.J., 2004, Controls on the strength of coupling among climate, erosion, and deformation in two-sided, frictional orogenic wedges at steady state: *Journal of Geophysical Research*, v. 109, F01011, <https://doi.org/10.1029/2003JF000019>.
- Willett, S.D., 1999, Orogeny and orography: The effects of erosion on the structure of mountain belts: *Journal of Geophysical Research*, v. 104, p. 28,957–28,981, <https://doi.org/10.1029/1999JB900248>.
- Willett, S., Beaumont, C., and Fullsack, P., 1993, Mechanical model for the tectonics of doubly vergent compressional orogens: *Geology*, v. 21, p. 371–374, [https://doi.org/10.1130/0091-7613\(1993\)021<0371:MMFTTO>2.3.CO;2](https://doi.org/10.1130/0091-7613(1993)021<0371:MMFTTO>2.3.CO;2).

Printed in USA